ADVANCED MATERIALS

DOI: 10.1002/adma.200701293

Mesoscopic Au "Meatball" Particles**

By *Hui Wang* and *Naomi J. Halas**

In this Communication we report the synthesis and optical properties of mesoscopic Au particles with a novel, highly roughened, "meatball-like" morphology, and the performance of these particles as substrates for surface-enhanced Raman spectroscopy (SERS). Sub-micrometer metallic particles of Au and Ag have unique optical properties in the visible and near infrared (NIR) regions of the spectrum that are highly useful for a variety of applications, such as nanoscale optical components or devices,[1–3] chemical and biomolecular sensing,[4,5] medical imaging and photothermal therapy,[6–8] and surface-enhanced spectroscopies.[9–11] The optical properties of metallic nanoparticles are dominated by the collective oscillations of free electrons in the metal, known as surface plasmons.[12] The plasmon resonance frequencies of a metallic nanoparticle are dependent on the particle's size, shape,[13,14] and surface topography because the oscillations of free electrons are controlled by the particle geometry.

For spherical Au or Ag nanoparticles much smaller than the wavelength of light, only the dipole plasmon resonance is excited. This size regime is known as the "dipole" or "quasistatic" limit, since all the electrons of the particle experience the same phase of the incident electromagnetic field.[15] As the particle size is increased, higher-order multipolar plasmon modes can also be excited, with the multipolar plasmon modes appearing at shorter wavelengths than the dipole plasmon feature in the particle's overall extinction spectrum. Since the excitation of higher-order modes occurs when the phase of the optical field varies across the spatial extent of the particle, they are also known as phase retardation effects. Phase retardation also gives rise to significant red-shifting and broadening of the dipole resonance. Higher-order multipolar plasmon modes have been theoretically predicted and experimentally observed for large Au or Ag quasispherical particles with diameters larger than 100 nm[16,17] and spherical metallic nanoshells.[18–21] For particles with reduced symmetry, or in an anisotropic dielectric environment, the nature of the multipolar plasmon modes becomes more complex. Metallic nanoparticles with nonspherical shapes, such as nanorods,[22] nanocubes,[23] triangular nanoprisms,[24] and nanopolyhedrons,[25] have also been shown to support higher-order multipolar plasmon modes.

In addition to particle size and shape, the surface topography of a particle can also significantly influence its optical properties. For example, recent studies have shown that the introduction of nanoscale texturing or the presence of defects on the nanoparticle surface can result in interesting changes to both the far-field and near-field properties of metallic nanoshells.[26,27] On macroscopic metallic surfaces or films, surface roughness and defects have long been known to relax the boundary conditions that prevent the direct excitation of surface plasmon waves. For mesoscopic particles, already in a size regime where direct optical excitation of dipole and higher-order multipole modes is possible, it is observed that the introduction of roughness onto the particle surface preferentially dampens the higher-order modes relative to those of a smooth spherical particle.[26,27] In general, roughened subwavelength particles are of great interest in light scattering studies, since a wide variety of naturally occurring particles, such as biological structures or atmospheric dust, have surfaces with nanoscale roughness. For metallic particles with rough surfaces, the enhanced local field is one mechanism that can contribute to the signal strength in surface-enhanced spectroscopies such as SERS.

Here we investigate the optical properties of sub-micrometer Au spheres with nanoscale surface roughness. These meatball-like Au particles were fabricated through controlled reduction of chloroauric acid by ascorbic acid in aqueous solution at room temperature. This approach is a modified protocol based on the fabrication procedure developed by Matijevic for polycrystalline Au microspheres[28] and by Van Blaaderen for large Ag colloids.[29] The colloidal meatball-like particles fabricated by this method exhibit nanoscale surface roughness (Fig. 1A), and also appear quite monodisperse, given their irregular surfaces. The size distribution reported in a histogram (Fig. 1B) was obtained from scanning electron microscopy (SEM) images of over 200 particles. The average particle size is 430 nm with a standard deviation of 38 nm. In Figure 1C, a SEM image with higher magnification is shown, revealing the surface topography of several individual particles. The surface of each particle is composed of a large number of randomly arranged, irregular nanoscale protrusions approximately 20–50 nm in size. Each particle appears to consist

[*] Prof. N. J. Halas, H. Wang
Department of Chemistry
Department of Electrical and Computer Engineering and the Laboratory for Nanophotonics (LANP), Rice University
6100 South Main St., Houston, TX 77005 (USA)
E-mail: halas@rice.edu

[**] This work was supported by Air Force Office of Scientific Research Grant F49620-03-C-0068, National Science Foundation (NSF) Grant EEC-0304097, National Aeronautics and Space Administration (NASA) Grant 68371, Robert A. Welch Foundation Grants C-1220, Army Research Office (ARO) Grant DAAD19-99-1-0315, and Multidisciplinary University Research Initiative (MURI) Grant W911NF-04-01-0203.

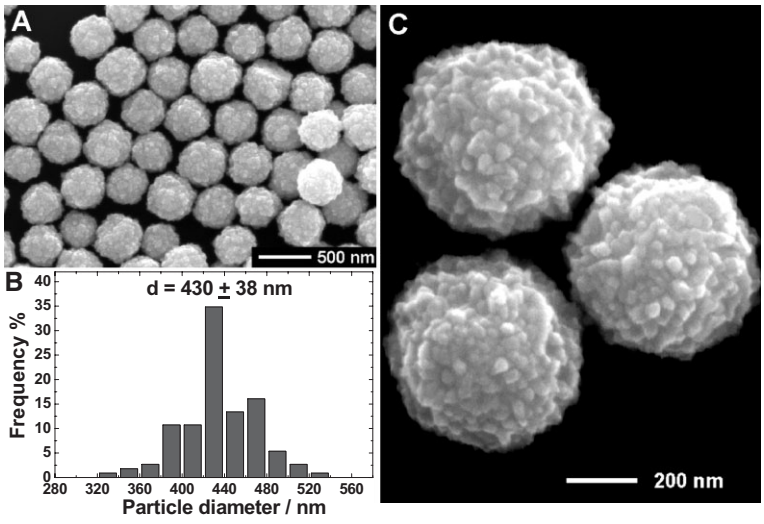

Figure 1. A) SEM image of the sub-micrometer meatball-like Au spheres with nanoscale surface roughness. B) Histograms indicating the particle size distribution. C) SEM image with higher resolution, revealing the surface topography of sub-micrometer Au particles.

of many nanometer-sized, crystalline subunits with well-defined grain boundaries. The polycrystalline structure of the particles arises from the subunit growth and aggregation that occur during the mild reduction of tetrachloroauric ions by ascorbic acid in the presence of gum Arabic as the dispersant. According to the particle growth model proposed by Matijevic[28] and Van Blaaderen,[29] a nucleation burst occurs once the concentration of the metal atoms reaches a critical supersaturation. Then the nucleation sites grow into nanoscale primary particles by diffusion capture of the remaining atoms. These primary particles then form aggregates, under appropriate reaction conditions, leading to the formation of larger spherical aggregates with a surprisingly narrow particle size distribution.

The optical properties of the meatball-like Au particles were investigated by visible-NIR extinction spectroscopy. Figure 2A shows the experimentally measured optical extinction spectrum of dilute colloidal particles homogenously dispersed in water. The monodispersity of the particles allows the experimental observation of well-defined higher-order multipole plasmon modes in addition to the dipole resonance. Several peaks corresponding to higher-order multipole resonances such as quadrupole and octupole can clearly be observed in the spectrum, while the dipole peak has been shifted into the infrared, beyond the scanning range, limited by water absorption beyond 1380 nm in wavelength for these samples. The two resolvable plasmon resonance peaks at ~ 925 nm and ~ 756 nm are identified as quadrupole and octupole resonances, respectively. These results are compared directly with theoretical calculations using Mie scattering theory for a spherical particle (430 nm in diameter) with perfectly smooth surface (Fig. 2B). The calculations were performed using the experimentally obtained dielectric function for Au[30] with a surrounding dielectric medium of water (n = 1.36). The calculated extinction is expressed as optical efficiency, which is the ratio of the energy scattered or absorbed by the nanoparticle to the energy incident on its physical cross section. The extinction of the sub-micrometer Au sphere is dominated by scattering. Only in the wavelength range near and below the onset of the Au interband transition (~ 520 nm) can a significant increase in the absorption efficiency be observed. When the experimental extinction of the rough particles is compared with the theoretical extinction of a smooth sphere of similar size, it is apparent that the higher-order multipolar resonances in the rough particles are significantly damped relative to the smooth particle predictions, and their plasmon frequencies are somewhat red-shifted. This higher-order mode dampening becomes more pronounced with increasing multipolar mode order: for a smooth Au sphere of this size, the predominant spectral feature is the hexadecapole mode, which appears to be entirely dampened in the experimental extinction spectrum of the rough particles.

The differences observed in resonance frequencies and spectral lineshapes between the experimental data and the theoretical calculations appear to be due directly to the presence of nanoscale roughness on the particle surface. Similar behavior was observed and analyzed theoretically, including detailed finite difference time domain simulations of light scattering directly from roughened particles, for Au nanoshells.[26,31] In the nanoshell case, while the dipolar nanoshell plasmon resonance in the extinction spectrum was observed to be robust with respect to surface roughness, the higher-order multipole resonances were seen to be significantly dampened as nanoscale roughness was increased, resulting in an overall red-shifting of the nanoshell spectral envelope. The dampening of the higher-order multipole resonances due to nanoscale particle surface roughness was also observed in angle-dependent light scattering measurements of roughened nanoshells, where the distinctive side lobes of the quadrupole scattering pattern were observed to be strongly suppressed.[27]

The Au particles were dispersed and immobilized onto poly(vinyl pyridine)-functionalized glass substrates.[32] Figure 3A shows the extinction spectrum of a sub-monolayer of dispersed particles immobilized on glass, in ambient air. The interparticle distance is larger than the diameter of particles, indicating that interparticle plasmon coupling should be minimal (Fig. 3B). In this case, the measured optical spectrum of these samples should be similar to the spectra obtainable from individual particles, blue-shifted relative to the same particles suspended in aqueous solution.[33] Three discernable plasmon resonance modes are observed, corresponding to the dipole (I), quadrupole (II), and octupole (III) resonances, respectively. The sensitivity of these plasmon features to the dielectric properties of the surrounding media[34] was examined by exposing these samples to solvents with varying refractive in-

ADVANCED MATERIALS

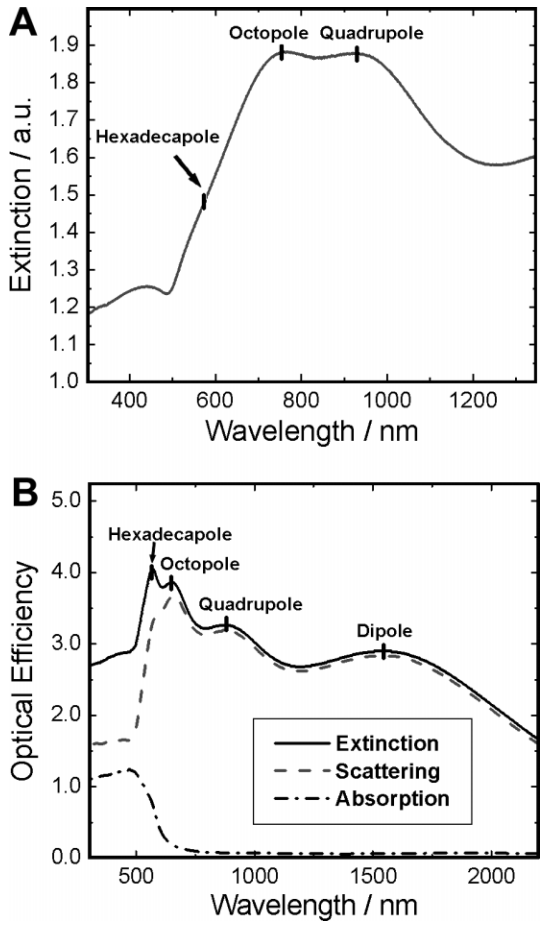

Figure 2. A) Experimentally measured extinction spectrum of the meatball-like Au particles dispersed in water. B) Theoretically calculated extinction (solid cure), scattering (dashed curve), and absorption (dashed-dotted curve) of a spherical Au particle (430 nm in diameter) with a smooth surface in water.

dices. As illustrated in Figure 3C, the dipole and all the higher-order multipole plasmon resonances progressively red-shift as the refractive index of the solvent is increased, with a linear dependence of plasmon wavelength on refractive index. The surface plasmon resonance (SPR) sensitivities of dipole, quadrupole, and octupole modes are determined to be 853.9 nm RIU^{-1}, 372.7 nm RIU^{-1}, and 299.1 nm RIU–1, respectively. The dipole and higher-order multipole plasmon modes of these meatball-like particles are quite sensitive to the dielectric properties of the surrounding medium relative to small Au nanoparticles. The plasmon resonance frequency becomes less sensitive to the surrounding medium for increasing multipolar order of the plasmon. This trend has also been observed previously for Au nanoshells[33] and Ag nanocubes.[23]

There are several general strategies for the construction of high-performance nanoengineered SERS substrates. One approach involves the positioning or fabrication of nearly adjacent metallic nanostructures with nanoscale gaps. Tiny gaps between adjacent metallic nanostructures have been shown to support extremely intense local electromagnetic fields upon plasmonic excitations,[35–41] providing "hot spots" with large SERS enhancements that approach single-molecule sensitivity for certain molecules. Another approach is based on the generation of optimized near-field enhancements on individual plasmonic nanoparticles, providing large field enhancement on open, exterior particle surface. This can be accomplished by controlled fabrication of nanoparticles with thin metallic shell layers,[42] sharp vertices,[40,43,44] nanoscale textured surfaces,[26] or nanostructures with reduced symmetry.[45,46] For isolated solid spherical Au nanoparticles with smooth surfaces, the SERS enhancements are reported to be pretty low, with the enhancement factors on the order of 10^3.[47] The localized near-field enhancements on the tip of nanoscale bumps or inside tiny cavities on the surface of meatball-like particles provide SERS enhancements that are significantly larger than those achievable on a solid spherical particle with a smooth surface. Surface roughness introduced onto nanoshells was also observed to increase their SERS enhancements.[26,42] Additionally, surface roughness increases the total surface area of the particles accessible to molecular adsorbates, which will also increase SERS signals.

The SERS performance of the meatball-like particle substrates was evaluated using *para*-mercaptoaniline (pMA) as the adsorbate. pMA is ideal for SERS quantification because it provides a strong SERS spectrum and forms self-assembled monolayers (SAMs) with a known packing density on Au surfaces. The Raman spectroscopic measurements were performed using a Renishaw microRaman spectrometer with a 785 nm diode laser as the excitation source. The laser beam size focused on the samples was 2 μm in diameter under confocal illumination. Figure 4A shows an optical microscopy image of a sub-monolayer of isolated particles dispersed on a glass slide used for these experiments. An SEM image of the same sample (Fig. 4B) shows a sparse particle distribution that ensures that only one particle is probed in each 2 μm diameter beam spot, indicating that SERS signals were obtained from individual particle substrates and were collected under the same experimental conditions. Figure 4C shows the SERS spectrum of pMA on individual Au particles (c), signals from bare Au particles (b), and normal Raman spectrum of pure pMA (a). (The broad feature centered at ~ 1380 cm^{-1} is due to a broad, weak fluorescence from a dopant in the glass substrate, and is subtracted from the SERS spectrum in (d).) The SERS spectra in Figure 4C are the averaged spectra of 15 scans over different particles with 20s acquisition time per scan. The peak intensities in the SERS spectra of pMA are highly reproducible on different particles with a standard deviation of less than 10 %. SERS enhancement factors were calculated by comparing ratios of the SERS peak intensity of saturated pMA SAMs to the corresponding unenhanced signals from neat pMA films of known thickness. The number of molecules being probed was estimated based on the surface area of each nanoparticle and packing density of pMA on the surface. Assuming that the surface area of each particle is approximately 10–100 times larger than that of a particle with the same size but completely smooth surface, the SERS en-

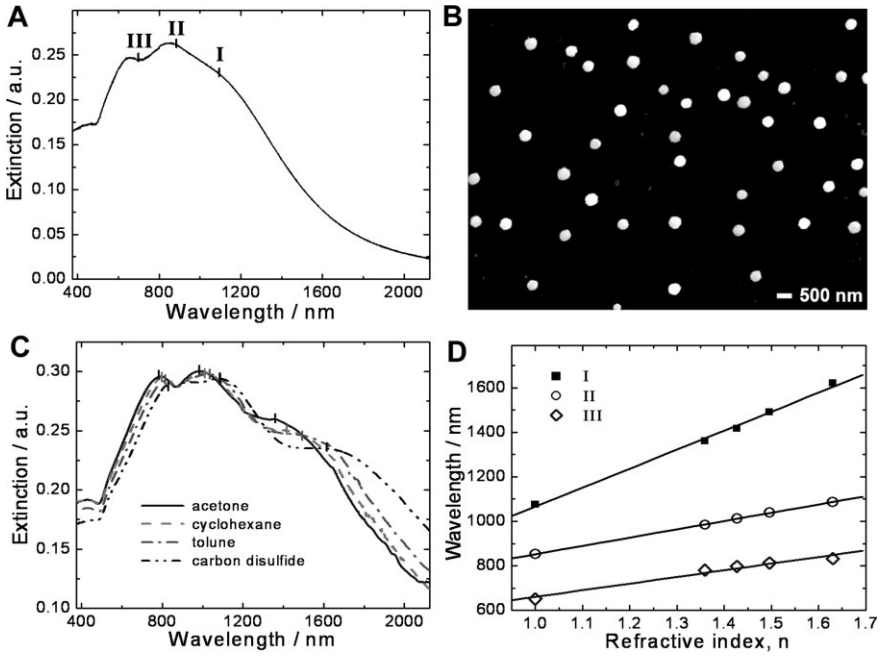

Figure 3. A) Extinction spectrum, and B) SEM image of a monolayer of isolated Au particles immobilized on a poly(vinylpyridine)-functionalized glass slide. C) Extinction spectra of the Au particle film immersed in different solvents, as indicated. D) Plasmon resonance wavelength as a function of solvent refractive index.

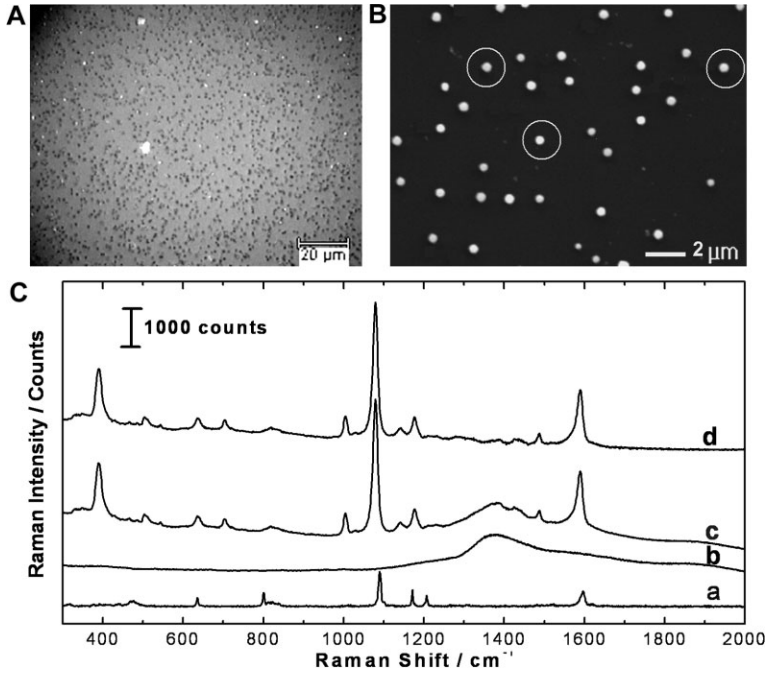

Figure 4. A) Optical microscope image and B) SEM image of isolated Au particles on a PVP-functionalized glass slide. The laser beam spot is 2 μm in diameter (represented by the circles superimposed on image). C) SERS of *para*-mercaptoaniline (pMA) on individual particles: a) Normal Raman spectrum of pure pMA, b) Raman spectrum collected from individual Au particles, c) SERS spectrum collected from individual Au particles with saturated pMA coverage, and d) SERS signals from pMA on the surface of individual Au particles (curve c subtracted by curve b). The SERS spectra shown here is an average of the SERS signal collected from 15 different individual particles.

hancement factors of pMA on these individual Au particles are estimated to be on the order of 10^6–10^7, which is several orders of magnitude higher than those achievable on smaller spherical Au nanoparticles with smooth outer surfaces. It should be noted that these enhancement factors represent the average enhancements over the whole surface of each particle, and that highly localized enhancements on the tips of the protrusions or inside the crevices of each particle's surface may be significantly larger than these measured enhancements.

These meatball-like Au particles can also self-assemble into multicrystalline close-packed arrays upon solvent evaporation. Figure 5A shows a SEM image of a monolayer close-packed particle array formed on glass. This array structure combines the features of both nanoscale roughness on the particle surface and the nanoscale interparticle junctions between neighboring particles. The plasmon interactions between the adjacent particles in this array structure not only dramatically modify the frequencies and lineshapes of the plasmon resonances relative to the individual, noninteracting particles, (see Fig. 5B), but also give rise to large field enhancements due to the interparticle gaps in addition to the electromagnetic enhancements inherent in the particles due to their rough surfaces. As evident in Figure 5C, the intensities of pMA SERS signals on the particle arrays increase dramatically by a factor of ~ 40 compared to the signals of pMA on individual particles. Such increases in SERS intensity arises from the increased number of particles being probed in the laser beam as well as the additional field enhancements in the interparticle gaps. The average enhancement factors over the surface of the arrays is estimated to be on the order of 10^7–10^8.

In conclusion, sub-micrometer meatball-like Au particles provide a very interesting mesoscopic regime in which their optical responses are determined by both the mesoscopic size and the particle's nanoscale surface roughness. Higher-order multipole plasmon modes that would be dominant for smooth Au particles in this size regime are significantly attenuated by nanoscale surface roughness. In contrast to small Au nanoparticles within the dipole limit, the dipole and higher-order multipole plasmon modes of the sub-micrometer Au spheres display increased SPR sensitivities to the dielectric properties of the surrounding medium.

ADVANCED MATERIALS

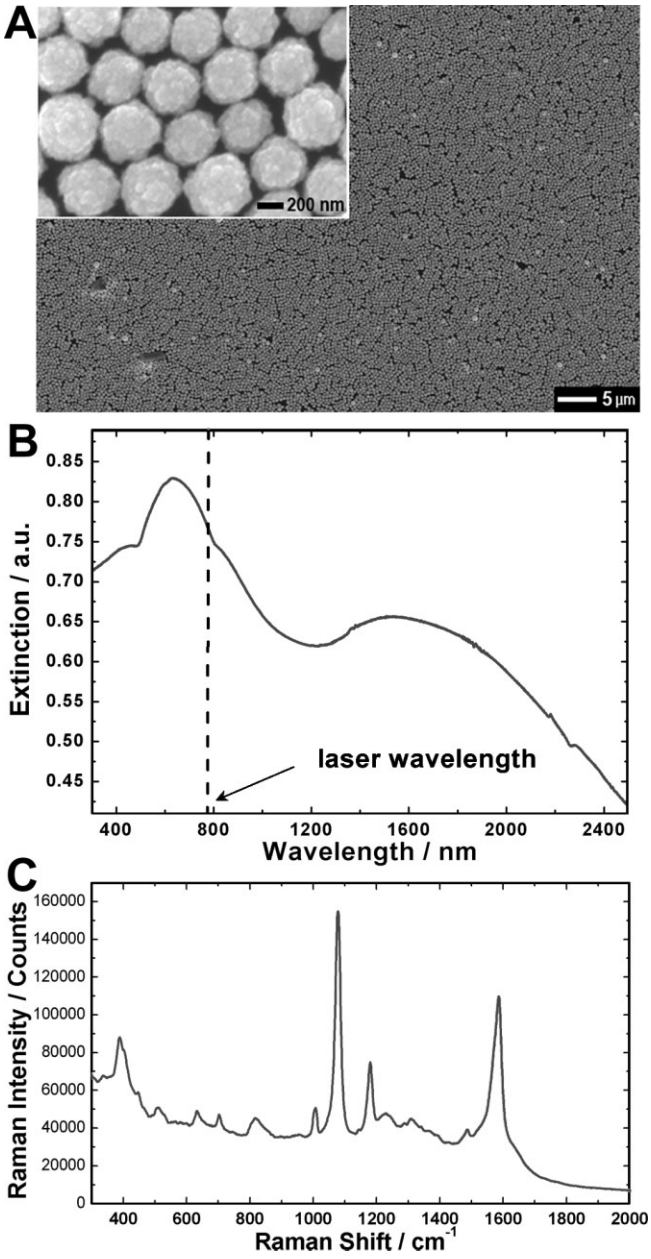

Figure 5. A) SEM image and B) extinction spectrum of a monolayer of close-packed submicrometer Au sphere arrays formed on a glass slide. The inset of panel A shows a higher resolution SEM image. C) SERS spectrum of pMA molecules on the Au particle arrays. The laser excitation wavelength is 785 nm, indicated in panel B.

The presence of nanoscale surface roughness significantly increases near-field enhancements on the particle surface, giving rise to stable and reproducible SERS enhancements on the order of 10^6–10^7 from individual particles. Close-packed arrays formed through the self-assembly of the sub-micrometer meatball-like particles combine the features of nanoscale surface roughness and the nanoscale interparticle junctions, resulting in SERS enhancements as large as ~ 10^8. The unique optical properties of these mesoscopic particles and particle arrays hold great potential in chemical sensing and spectroscopic applications.

Experimental

Tetrachloroauric acid, L-ascorbic acid, gum Arabic, poly(4-vinyl pyridine) (PVP), and *para*-mercaptoaniline (pMA) were purchased from Sigma–Aldrich. 200-proof ethanol was obtained from Fisher Scientific (Hampton, NH). Ultrapure water (18.2 MΩ resistivity) was obtained using a Milli-Q water purification system (Millipore, Billerica, MA). Glass microscope slides were purchased from Gold Seal Products (Portsmouth, NH).

The particles were fabricated through controlled reduction of chloroauric acid by ascorbic acid in aqueous solution at room temperature using gum Arabic as the stabilizer. In a typical procedure, 25 mL of aqueous solution containing 100 mM L-ascorbic acid and 0.2 wt % gum Arabic was introduced dropwise into 25 mL of aqueous solution containing 20 mM tetrachloroauric acid and 0.2 wt % gum Arabic under vigorous stirring conditions. The introduction of the ascorbic acid solution into the tetrachloroauric acid solution was accomplished within 3 min. The solution was then stirred for 30 min at room temperature. The resulting Au colloidal solution was brownish in color. The Au particles were centrifuged and redispersed in water three times to remove the excess reactants in the solution. The colloidal particles were finally dispersed in 10 mL of water.

The sub-monolayer films of isolated Au meatball-like particles were prepared by immobilizing the particles onto PVP-functionalized glass. Briefly, glass slides were cleaned in piranha solution (sulfuric acid:hydrogen peroxide, 7:3) and immersed in a 1 % wt. solution of PVP in ethanol for 24 h. (***Caution**: Piranha solution reacts violently with organic matter and should be handled with extreme care!*) The slides were rinsed thoroughly with ethanol and dried with N_2 gas, then immersed in an aqueous solution of particles for a certain period of time. The coverage of the Au particles on the glass surface increases with immersion time until a saturated coverage of isolated particles was reached, after approximately 1 h. Upon removal from the colloidal particle solution, the films were rinsed thoroughly with ethanol and dried with N_2.

Assembly of the particles into close-packed arrays was accomplished by depositing a droplet of the colloidal solution (30 μL) on a substrate surface (glass slide, silicon wafer, or ITO glass), and allowing it dry undisturbed under ambient conditions.

The samples for SERS measurements were prepared by evaporating 10 μL of a 20 μM solution of pMA in ethanol on the surface of the isolated particles or the close-packed particle arrays. Raman spectra were obtained with a Renishaw micro-Raman spectrometer using a 785 nm excitation laser (250 mW), confocal mode (beam size 2 μm in diameter), 50× objective, 0.5 % laser power, and an acquisition time of 20 s. The laser power focused on the samples was measured to be 3.5 mW when the 50× objective and 0.5 % laser power were used. Extinction spectra were obtained using a Cary 5000 UV/Vis/NIR spectrophotometer in the wavelength range of 400 nm to 2400 nm. SEM measurements were performed on a Phillips FEI XL-30 environmental scanning electron microscope.

Received: May 28, 2007
Revised: September 13, 2007
Published online: January 29, 2008

[1] J. B. Pendry, *Phys. Rev. Lett.* **2000**, *85*, 3966.
[2] S. A. Maier, M. L. Brongersma, P. G. Kik, S. Meltzer, A. A. G. Requicha, H. A. Atwater, *Adv. Mater.* **2001**, *13*, 1501.
[3] W. L. Barnes, A. Dereux, T. W. Ebbesen, *Nature* **2003**, *424*, 824.
[4] R. Elghanian, J. J. Storhoff, R. C. Mucic, R. L. Letsinger, C. A. Mirkin, *Science* **1997**, *277*, 1078.
[5] A. J. Haes, R. P. Van Duyne, *Anal. Bioanal. Chem.* **2004**, *379*, 920.

[6] L. R. Hirsch, R. J. Stafford, J. A. Bankson, S. R. Sershen, B. Rivera, R. E. Price, J. D. Hazle, N. J. Halas, J. L. West, *Proc. Natl. Acad. Sci. USA* **2003**, *100*, 13549.

[7] C. Loo, A. Lowery, N. Halas, J. West, R. Drezek, *Nano Lett.* **2005**, *5*, 709.

[8] X. H. Huang, I. H. El-Sayed, W. Qian, M. A. El-Sayed, *J. Am. Chem. Soc.* **2006**, *128*, 2115.

[9] K. Kneipp, H. Kneipp, I. Itzkan, R. R. Dasari, M. S. Feld, *Chem. Rev.* **1999**, *99*, 2957.

[10] S. Nie, S. R. Emory, *Science* **1997**, *275*, 1102.

[11] Y. W. C. Cao, R. C. Jin, C. A. Mirkin, *Science* **2002**, *297*, 1536.

[12] U. Kreibig, M. Vollmer, *Optical Properties of Metal Clusters*, Springer, Berlin, Germany **1995**.

[13] E. Prodan, P. Nordlander, *Nano Lett.* **2003**, *3*, 543.

[14] E. Prodan, P. Nordlander, *J. Chem. Phys.* **2004**, *120*, 5444.

[15] C. F. Bohren, D. R. Huffman, *Absorption and Scattering of Light by Small Particles*, Wiley, New York **1998**.

[16] J. Rodriguez-Fernandez, J. Perez-Juste, F. J. G. de Abajo, L. M. Liz-Marzan, *Langmuir* **2006**, *22*, 7007.

[17] A. S. Kumbhar, M. K. Kinnan, G. Chumanov, *J. Am. Chem. Soc.* **2005**, *127*, 12444.

[18] S. J. Oldenburg, J. B. Jackson, S. L. Westcott, N. J. Halas, *Appl. Phys. Lett.* **1999**, *75*, 2897.

[19] S. J. Oldenburg, R. D. Averitt, S. L. Westcott, N. J. Halas, *Chem. Phys. Lett.* **1998**, *288*, 243.

[20] J. B. Jackson, N. J. Halas, *J. Phys. Chem. B* **2001**, *105*, 2743.

[21] H. Wang, F. Tam, N. K. Grady, N. J. Halas, *J. Phys. Chem. B* **2005**, *109*, 18218.

[22] E. K. Payne, K. L. Shuford, S. Park, G. C. Schatz, C. A. Mirkin, *J. Phys. Chem. B* **2006**, *110*, 2150.

[23] L. J. Sherry, S. H. Chang, G. C. Schatz, R. P. Van Duyne, B. J. Wiley, Y. N. Xia, *Nano Lett.* **2005**, *5*, 2034.

[24] J. E. Millstone, S. Park, K. L. Shuford, L. D. Qin, G. C. Schatz, C. A. Mirkin, *J. Am. Chem. Soc.* **2005**, *127*, 5312.

[25] A. Tao, P. Sinsermsuksakul, P. D. Yang, *Angew. Chem. Int. Ed.* **2006**, *45*, 4597.

[26] H. Wang, G. P. Goodrich, F. Tam, C. Oubre, P. Nordlander, N. J. Halas, *J. Phys. Chem. B* **2005**, *109*, 11083.

[27] H. Wang, K. Fu, R. A. Drezek, N. J. Halas, *Appl. Phys. B* **2006**, *84*, 191.

[28] D. V. Goia, E. Matijevic, *New J. Chem.* **1998**, *22*, 1203.

[29] K. P. Velikov, G. E. Zegers, A. van Blaaderen, *Langmuir* **2003**, *19*, 1384.

[30] P. B. Johnson, R. W. Christy, *Phys. Rev. B* **1972**, *6*, 4370.

[31] C. Oubre, P. Nordlander, *J. Phys. Chem. B* **2004**, *108*, 17740.

[32] S. Malynych, I. Luzinov, G. Chumanov, *J. Phys. Chem. B* **2002**, *106*, 1280.

[33] F. Tam, C. E. Moran, N. J. Halas, *J. Phys. Chem. B* **2004**, *108*, 17290.

[34] E. Prodan, A. Lee, P. Nordlander, *Chem. Phys. Lett.* **2002**, *360*, 325.

[35] K. Kneipp, Y. Wang, H. Kneipp, L. T. Perelman, I. Itzkan, R. R. Dasari, M. S. Feld, *Phys. Rev. Lett.* **1997**, *78*, 1667.

[36] A. M. Michaels, M. Nirmal, L. E. Brus, *J. Am. Chem. Soc.* **1999**, *121*, 9932.

[37] H. X. Xu, E. J. Bjerneld, M. Kall, L. Borjesson, *Phys. Rev. Lett.* **1999**, *83*, 4357.

[38] H. Wang, C. S. Levin, N. J. Halas, *J. Am. Chem. Soc.* **2005**, *127*, 14992.

[39] S. J. Lee, A. R. Morrill, M. Moskovits, *J. Am. Chem. Soc.* **2006**, *128*, 2200.

[40] D. P. Fromm, A. Sundaramurthy, A. Kinkhabwala, P. J. Schuck, G. S. Kino, W. E. Moerner, *J. Chem. Phys.* **2006**, *124*, 061101.

[41] C. Oubre, P. Nordlander, *J. Phys. Chem. B* **2005**, *109*, 10042.

[42] C. E. Talley, J. B. Jackson, C. Oubre, N. K. Grady, C. W. Hollars, S. M. Lane, T. R. Huser, P. Nordlander, N. J. Halas, *Nano Lett.* **2005**, *5*, 1569.

[43] H. Wang, D. W. Brandl, F. Le, P. Nordlander, N. J. Halas, *Nano Lett.* **2006**, *6*, 827.

[44] E. Hao, G. C. Schatz, *J. Chem. Phys.* **2004**, *120*, 357.

[45] H. Wang, Y. Wu, B. Lassiter, C. Nehl, J. H. Hafner, P. Nordlander, N. J. Halas, *Proc. Natl. Acad. Sci. USA* **2006**, *103*, 10856.

[46] Y. Lu, G. L. Liu, J. Kim, Y. X. Mejia, L. P. Lee, *Nano Lett.* **2005**, *5*, 119.

[47] Z. Zhu, T. Zhu, Z. Liu, *Nanotechnology* **2004**, *15*, 357.